

Full-dimensional multilayer multiconfigurational time-dependent Hartree study of electron transfer dynamics in the anthracene/C60 complex

Yu Xie, Jie Zheng, and Zhenggang Lan

Citation: *The Journal of Chemical Physics* **142**, 084706 (2015); doi: 10.1063/1.4909521

View online: <http://dx.doi.org/10.1063/1.4909521>

View Table of Contents: <http://scitation.aip.org/content/aip/journal/jcp/142/8?ver=pdfcov>

Published by the AIP Publishing

Articles you may be interested in

A full-dimensional multilayer multiconfiguration time-dependent Hartree study on the ultraviolet absorption spectrum of formaldehyde oxide

J. Chem. Phys. **141**, 124309 (2014); 10.1063/1.4896201

Reaction dynamics with the multi-layer multi-configurational time-dependent Hartree approach: $\text{H} + \text{CH}_4 \rightarrow \text{H}_2 + \text{CH}_3$ rate constants for different potentials

J. Chem. Phys. **137**, 244106 (2012); 10.1063/1.4772585

Full dimensional quantum-mechanical simulations for the vibronic dynamics of difluorobenzene radical cation isomers using the multilayer multiconfiguration time-dependent Hartree method

J. Chem. Phys. **137**, 134302 (2012); 10.1063/1.4755372

Proton transfer reactions in model condensed-phase environments: Accurate quantum dynamics using the multilayer multiconfiguration time-dependent Hartree approach

J. Chem. Phys. **127**, 144503 (2007); 10.1063/1.2772265



All mode dynamics at the conical intersection of an octa-atomic molecule: Multi-configuration time-dependent Hartree (MCTDH) investigation on the butatriene cation

J. Chem. Phys. **115**, 2088 (2001); 10.1063/1.1384872



AIP | The Journal of
Chemical Physics

Meet The New Deputy Editors

	Peter Hamm		David E. Manolopoulos		James L. Skinner
---	-------------------	---	------------------------------	---	-------------------------

Full-dimensional multilayer multiconfigurational time-dependent Hartree study of electron transfer dynamics in the anthracene/C60 complex

Yu Xie,^{1,2} Jie Zheng,^{1,2} and Zhenggang Lan^{1,2,a)}

¹CAS Key Laboratory of Biobased Materials, Qingdao Institute of Bioenergy and Bioprocess Technology, Chinese Academy of Sciences, Qingdao 266101, China

²University of Chinese Academy of Sciences, Beijing 100049, People's Republic of China

(Received 10 November 2014; accepted 5 February 2015; published online 27 February 2015)

Electron transfer at the donor-acceptor heterojunctions plays a critical role in the photoinduced process during the solar energy conversion in organic photovoltaic materials. We theoretically investigate the electron transfer process in the anthracene/C60 donor-acceptor complex by using quantum dynamics calculations. The electron-transfer model Hamiltonian with full dimensionality was built by quantum-chemical calculations. The quantum dynamics calculations were performed using the multiconfigurational time-dependent Hartree (MCTDH) theory and multilayer (ML) MCTDH methods. The latter approach (ML-MCTDH) allows us to conduct the comprehensive study on the quantum evolution of the full-dimensional electron-transfer model including 4 electronic states and 246 vibrational degrees of freedom. Our quantum dynamics calculations exhibit the ultrafast anthracene \rightarrow C60 charge transfer process because of the strong coupling between excitonic and charge transfer states. This work demonstrates that the ML-MCTDH is a very powerful method to treat the quantum evolution of complex systems. © 2015 AIP Publishing LLC. [<http://dx.doi.org/10.1063/1.4909521>]

I. INTRODUCTION

Organic solar cells (OSCs) are potential alternatives for silica-based photovoltaic systems due to their advantages such as simple processing, low costs, etc.^{1–3} So far, organic photovoltaic devices based on the bulk heterojunctions (BHJs) seem to be very promising with their rapid increasing of the energy conversion efficiencies.^{3,4} The solar energy conversion of OSC devices is initialized by a series of primary photoreactions in the BHJ heterojunctions. After photoabsorption, the excitonic states of donor materials are generated by sunlight. Then, the excitons are separated into the weakly coupled holes and electrons at the heterojunctions, resulting in the so-called photo-induced electron transfer (ET) processes from donor to acceptor materials. Therefore, the ET processes are certainly key steps for the photonic-electric energy conversion in OSCs.^{1–3}

In last decades, extensive experimental studies were dedicated to explore the photo-induced electron transfer processes in OSCs.^{2,5–17} Recently, many time-resolved studies figured out that the photo-induced ET processes are far more complex than the traditional point of view, since they may occur on an ultrafast time scale, about 50 ~ 200 fs.^{2,5–9} These fast ET processes imply the strong coupling between electron donors and acceptors. In addition, such ultrafast ET processes should essentially be the nonadiabatic dynamics that involves the strong coupled nuclear-electronic motion. The understanding of the ultrafast ET in OSC represents the great challenging in theoretical chemistry, owing to the invalidity of the Born-Oppenheimer approximation.

In last decades, various theoretical approaches were employed to describe the ultrafast ET process in complex systems.^{18–43} The widely used Marcus theory²⁶ may provide preliminary understandings, while the ultrafast ET is beyond its treatable limit. Several sophisticated approaches were proposed based on the quantum dissipative theories in the framework of reduced density matrix, such as the Redfield equation,⁴⁴ generalized Bloch-Redfield equation,²¹ and the hierarchy-equation-of-motion (HEOM) methods.^{22,45–47} As a perturbation theory, the Redfield equation can only describe the weak coupling between system (electronic motion) and bath (nuclear motion) properly. The HEOM method is regarded as an “exact” method in some sense, but it is computationally very expensive.^{22,45–47} Alternatively, several groups advocated the mix-quantum-classical approaches,^{39–42,48–50} which seem to be very attractive and practical due to the simplicity of numerical implementation. For instance, the surface hopping method^{51–53} is very popular in the treatment of the ultrafast ET dynamics,^{39–42} but it suffers from many problems,^{54–57} such as incorrect coherence, internal inconsistency, and frustrated hops. In last few years, the real-time TDDFT (time-dependent density functional theory) method^{25,37,43} received the great attention since it offers a simple physical picture to view ET processes via the time-dependent electronic density. Some efforts were also made to combine the real-time TDDFT with the Ehrenfest dynamics.²⁵ However, it is not trivial to derive the force acting on the nuclei due to the non-stationary feature of electronic density in the real-time TDDFT. In addition, the mean-field Ehrenfest dynamics also suffers from many deficiencies, such as the wrong description of coherence. Although the quantum-classical Liouville equation provides the better description

a)lanzg@qibebt.ac.cn

of electronic motion, the numerical instability prevents its broad applications.^{58,59} A few of approaches with more rigorous semiclassical approximation, such as initial value representation (IVR) method^{58–60} and symmetrical quasi-classical (SQC) method,³⁸ display their excellent ability to recover quantum effects in the dynamics simulations, while their further application is hindered by the large computational cost and the low numerical stability for the long-time propagation. Moreover, the ultrafast ET processes of complex systems may also be described by stochastic approaches, such as recently developed time-dependent wavepacket diffusion (TDWPD) method,^{32,33} while the numerical stability may be strongly dependent on the system under investigation. Thus until now, all methods show advantages and shortcomings.

Certainly, one way to understand the ultrafast ET processes in complex system is to return to the quantum dynamics simulations. In last two decades, the so-called multi-configuration time-dependent Hartree (MCTDH) method received the great attention,^{61,62} which provides a numerical way to solve the time-dependent Schrödinger equation exactly with high efficiency under the suitable Hamiltonian. This method gives us the possibility to provide the full quantum treatment for the nonadiabatic dynamics of complex systems with high accuracy. Until now, the MCTDH approach was successfully employed in the ET processes in OSCs up to tens of vibrational modes,^{19,20,63} while normally much larger degrees of freedom (DOFs) may be involved for the more complex systems.

As a powerful extension of the standard MCTDH approach, multilayer (ML) MCTDH can deal with thousands degrees of freedom.¹³ The ML-MCTDH theory was first formulated by Wang and Thoss, who provided an implementation of this method for three layers initially. Later on, they extended this approach up to four layers and showed its applicability on the ET processes in dye-semiconductor systems.^{13–17} At the same time, Meyer and Worth also independently provided a formally identical formulation termed as “cascading MCTDH,” but without any implementation.⁶⁴ Manthe provided a recursive formulation of the ML-MCTDH equations of motion (EOMs), which in principle extends the cascading expansion up to the infinite number of layers.^{65,66} Importantly, this approach shows an efficient way to construct the EOM for each layer and largely reduced the coding difficulty in the ML-MCTDH implementation. According to this idea, ML-MCTDH was successfully implemented into the Heidelberg MCTDH package by Meyer and co-workers, which allows the large-scaled ML-MCTDH calculation on the quantum evolution of extremely complex systems.^{67–70}

In this contribution, we chose the anthracene/C60 complex as a simplified model system to investigate the ET process at the donor-acceptor heterojunctions. To investigate the influence of the nuclear degrees of freedom on the ET process, the full dimensional (all the 246 vibrational modes) quantum dynamics of the 4 relevant donor/acceptor electronic states were carried out within the framework of ML-MCTDH using the Heidelberg MCTDH package.⁷⁰ The reduced-dimensionality models were also investigated to examine the different performances of MCTDH and ML-MCTDH. The diabatic model Hamiltonian was built

employing the projection-operator approach and electronic-structure calculations. This work represents our initial efforts to employ the ML-MCTDH to deal with the ET processes of complex OSC systems.

This article is organized as follows: in Sec. II, theoretical methods are introduced, including the construction of the diabatic ET Hamiltonian, electronic-structure calculations and quantum dynamics, etc. Results and discussion are given in Sec. III. After that, our conclusion is presented in Sec. IV.

II. THEORY AND METHODS

A. Diabatic ET Hamiltonian

The diabatic model Hamiltonian based on the *ab initio* calculations was built to study the anthracene (An) → fullerene (C60) ET process. In a donor-acceptor complex, a photogenerated excitonic donor state (An⁺-C60, henceforth denoted $|\psi_d\rangle$) is coupled to several charge separated acceptor states (An⁺-C60⁻, henceforth denoted $|\psi_a\rangle$). The Hamiltonian reads

$$H = T_{nuc} + |\psi_d\rangle V_{dd} \langle\psi_d| + \sum_a |\psi_a\rangle V_{aa} \langle\psi_a| + \sum_a (|\psi_d\rangle V_{da} \langle\psi_a| + |\psi_a\rangle V_{ad} \langle\psi_d|), \quad (2.1)$$

where V_{dd} and V_{aa} denote the energies of the electronic donor and acceptor states, respectively. The off-diagonal matrix elements $V_{da}(V_{ad})$ characterize the donor-acceptor couplings. T_{nuc} denotes the kinetic energy of the nuclear degrees of freedom.

Following previous theoretical approaches, we considered small nuclear displacements and took the normal mode approximation. The equilibrium geometry of the electronic ground state was taken as reference geometry. For simplicity, the dimensionless normal coordinates Q_i ⁷¹ with associated frequencies ω_i were employed to represent the diagonal elements of the diabatic Hamiltonian, namely,^{14,15,17,19,20,72}

$$V_{dd} = E_d + \frac{1}{2} \sum_i \omega_i Q_i^2 + \sum_i \kappa_i^{(d)} Q_i, \quad (2.2a)$$

$$V_{aa} = E_a + \frac{1}{2} \sum_i \omega_i Q_i^2 + \sum_i \kappa_i^{(a)} Q_i, \quad (2.2b)$$

where E_d and E_a are energies of the donor and acceptor electronic states, respectively, at the reference geometry. The $\kappa_i^{(n)}$ ($n = d, a$) are the gradients of the potential energy functions at the reference geometry and they represent the first-order intra-state vibronic couplings. The current approach neglects the frequency shift and the Dushinsky rotation of the normal modes.

Several previous works^{14,16,20} recommended to represent the D-A couplings by their zero-order inter-state couplings, namely,

$$V_{da} = V_{ad} = \lambda_{da}, \quad (2.3)$$

since they should already capture the leading contribution.

B. Determination of the parameters in diabatic Hamiltonian

The parameters in the diabatic Hamiltonian (Eqs. (2.1)–(2.3)) were determined from the electronic-structure calculations using the projection-operator approach,⁷³ which was used in the treatment of the ET processes of dye-semiconductor systems by Wang, Thoss, and their co-workers.^{14–16,72} This approach is proven to be very useful and practical in the construction of the diabatic Hamiltonian in the description of the ET processes of complex systems. As this method was comprehensively discussed in previous works,^{14–16,72} only a brief description is provided here.

In many previous works, the eigenstate energies of the one-electron wave functions (i.e., molecular orbitals (MOs)), in particular some frontier orbitals, were often selected to construct the energy-level diagrams for electronic devices.^{14–16} Thus, within the framework of the single-electron picture, the ET process can be viewed as the electron injection from the localized LUMO of An to the localized low-lying virtual orbitals of C60, which define the donor and acceptor states $|\psi_d\rangle$ (An⁺-C60) and $|\psi_a\rangle$ (An⁺-C60[−]), respectively. According to this idea, the diabatic Hamiltonian was constructed by the manipulation of the Fock matrix that was obtained from the electronic-structure calculations of the donor-acceptor complexes.^{14–16,72}

We separate the An/C60 complex into two parts: the donor part (An) and the acceptor part (C60). In principle, the atomic orbitals (AOs) are also well divided into two groups according to their locations. The donor group ($|\varphi_j^d\rangle$) consists of the AOs centered at the atoms of An, while the acceptor group ($|\varphi_j^a\rangle$) contains the AOs centered at the atoms of C60.

The set of atomic orbitals ($|\varphi_j^d\rangle, |\varphi_j^a\rangle$) of the whole system is then orthogonalized according to the Löwdin transformation,^{74–77}

$$|\tilde{\varphi}_n\rangle = \sum_j (S^{-1/2})_{jn} |\varphi_j\rangle, \quad (2.4)$$

where S denotes the AO overlap matrix with elements ($S_{kl} = \langle \varphi_k | \varphi_l \rangle$). Since such transformation largely keeps the localization feature of the new basis functions, the separation of the donor ($|\tilde{\varphi}_n^d\rangle$) and acceptor ($|\tilde{\varphi}_n^a\rangle$) orbitals is still valid. The Fock matrix in the Löwdin orthogonal basis becomes

$$\tilde{\mathbf{F}} = \mathbf{S}^{-1/2} \mathbf{F} \mathbf{S}^{-1/2}, \quad (2.5)$$

where \mathbf{F} denotes the Fock matrix in the original AO basis. Such Fock matrix can be arranged in the following donor-acceptor block structure

$$\tilde{\mathbf{F}} = \begin{pmatrix} \tilde{\mathbf{F}}_{dd} & \tilde{\mathbf{F}}_{da} \\ \tilde{\mathbf{F}}_{ad} & \tilde{\mathbf{F}}_{aa} \end{pmatrix}. \quad (2.6)$$

Next, the two (donor and acceptor) blocks $\tilde{\mathbf{F}}_{\alpha\alpha}$ ($\alpha = d, a$) of the Fock matrix are individually diagonalized via

$$\tilde{\mathbf{F}}_{\alpha\alpha} = \mathbf{D}_{\alpha}^{\dagger} \tilde{\mathbf{F}}_{\alpha\alpha} \mathbf{D}_{\alpha}, \quad (2.7)$$

and the off-diagonal blocks become

$$\tilde{\mathbf{F}}_{\alpha\beta} = \mathbf{D}_{\alpha}^{\dagger} \tilde{\mathbf{F}}_{\alpha\beta} \mathbf{D}_{\beta}. \quad (2.8)$$

Thus, the prediagonalized block structure of the Fock matrix reads

$$\tilde{\mathbf{F}} = \begin{pmatrix} \tilde{\mathbf{F}}_{dd} & \tilde{\mathbf{F}}_{da} \\ \tilde{\mathbf{F}}_{ad} & \tilde{\mathbf{F}}_{aa} \end{pmatrix} = \begin{pmatrix} \varepsilon_{1,d} & 0 & \cdots & & \\ 0 & \varepsilon_{2,d} & \cdots & & \\ \vdots & \vdots & \ddots & & \\ & & & \varepsilon_{1,a} & 0 & \cdots \\ & & & 0 & \varepsilon_{2,a} & \cdots \\ & & & \vdots & \vdots & \ddots \end{pmatrix}. \quad (2.9)$$

This way gives the localized molecular orbitals (LMOs, $|\tilde{\varphi}_j^{\alpha}\rangle$) of donor and acceptor, namely,

$$|\tilde{\varphi}_n^{\alpha}\rangle = \sum_j (D_{\alpha})_{jn} |\tilde{\varphi}_j^{\alpha}\rangle. \quad (2.10)$$

Two diagonal blocks of the Fock matrix (Eq. (2.10)) with indices d and a denote the energies of the localized donor and acceptor states, respectively. The off-diagonal blocks contain the diabatic coupling elements.

In this paper, we only considered the single donor state $|\psi_d\rangle$ representing the LUMO of the donor part, while several acceptor states $|\psi_a\rangle$ (unoccupied orbitals of the acceptor part) were chosen in the case of their energies close to that of the donor state. Thus, the diabatic Hamiltonian elements were given by $V_{dd} = \varepsilon_{d,n}$, $V_{kk} = \varepsilon_{a,k}$, and $V_{dk} = \tilde{F}_{da,nk}$ ($\tilde{F}_{da,nk}$ are the elements of the off-diagonal blocks), respectively.

As a short summary, all parameters in diabatic Hamiltonian (Eqs. (2.1)–(2.3)) were readily obtained based on the electronic structure calculations. ω_i was directly obtained from the normal mode analysis of the overall system. E_d , E_k , and V_{dk} were obtained from the prediagonalized block Fock matrix. $\kappa_i^{(d)}$ and $\kappa_i^{(a)}$ were obtained from the gradients of the donor and acceptor states at the equilibrium geometry of the overall system.

C. Electronic structures

The electronic structure of anthracene/fullerene calculations were performed with the density functional theory (DFT) method at the PBE/SVP (Perdew-Burke-Ernzerhof functional and split-valence plus polarization basis set) level using the Turbomole program.⁷⁸ The multipole-accelerated RI-J (the Resolution of the Identity approximation for the Coulomb potential) approximation (MARI-J)⁷⁹ was used in the geometry optimization, by which the computational cost is dramatically reduced without loss of accuracy.

To estimate the influence of the DFT functionals on the ET dynamics of the anthracene/C60 complex, we also performed further electronic-structure calculations with the B3LYP (Becke, three-parameter, Lee-Yang-Parr exchange-correlation) functional and the SVP basis set using Turbomole program⁷⁸ and the long range-corrected functional LC- ω PBE/6-31G* using Gaussian 09 program.⁸⁰ The ML-MCTDH results with electronic structures calculated using these functionals are given in the supplementary material.⁸¹

D. Quantum dynamics

In this section, we illustrate our procedure to perform quantum dynamics. All MCTDH and ML-MCTDH calculations were performed by using the Heidelberg MCTDH package.⁷⁰

In order to determine which acceptor states play major roles in the ET process, we first took several unoccupied LMOs of acceptor (energetically close to the donor state) as the acceptor states to study the pure electronic dynamics without the inclusion of the nuclear motion. Next, we only took three acceptor states in the further treatment on the coupled-nuclei-electrons dynamics, since only they show the large contribution in the pure ET dynamics (see below for details).

The two-state (2S) model was first examined, which includes one donor state and one acceptor state (one of the three selected ones). In this step, the reduced dimensional models with several vibrational degrees of freedom were treated by MCTDH and ML-MCTDH for comparison. As our first efforts to utilize MCTDH and ML-MCTDH to study the quantum evolution of complex systems, the standard wave-packet propagation method was also used to simulate the 2S-2D (2 electronic states, 2 vibrational degrees of freedom) model for comparison to make sure the correct employment of MCTDH and ML-MCTDH. When a lot of the vibrational degrees of freedom were involved, MCTDH cannot give converged results and only ML-MCTDH method was utilized in these cases.

Finally, the full quantum evolution of the ET process was investigated within a completed model including 4 electronic states and 246 modes (all vibrations) using the ML-MCTDH method.

1. Wave-packet propagation method

Following the standard way, the wave-packet were propagated using split-operator (SO) method.⁸² We employed the fast Fourier transform (FFT) method⁸³ to evaluate the propagation of the nuclear kinetic energy operator. In the current 2S-2D model, the grid for the wave-packet propagation consists of 128 points (from -14.0 to 14.0) for each vibrational coordinate. The wave-packets are propagated for 120 fs with a time step of 0.05 fs.

2. MCTDH

In contrast to the standard quantum dynamics method, the MCTDH method^{64,84} uses the time-dependent basis to represent the wave function. For a system with f DOFs described by coordinates Q_1, \dots, Q_f , the following *ansatz* is applied:

$$\Psi(Q_1, \dots, Q_f, t) = \sum_{j_1=1}^{n_1} \cdots \sum_{j_f=1}^{n_f} A_{j_1 \dots j_f}(t) \prod_{\kappa=1}^f \varphi_{j_\kappa}^{(\kappa)}(Q_\kappa, t). \quad (2.11)$$

Here, $A_{j_1 \dots j_f}$ denote the time dependent expansion coefficients and $\{\varphi_{j_\kappa}^{(\kappa)}\}$ denote the time-dependent basis functions, known as single particle functions (SPFs). Applying the variational principle

$$\left\langle \delta \Psi \left| H - i \frac{\partial}{\partial t} \right| \Psi \right\rangle = 0, \quad (2.12)$$

the coupled equations of motion are obtained as

$$i \frac{\partial}{\partial t} A_{j_1 \dots j_f} = \sum_{l_1 \dots l_f} \left\langle \prod_{\kappa=1}^f \varphi_{j_\kappa}^{(\kappa)} \left| H \right| \prod_{\kappa=1}^f \varphi_{l_\kappa}^{(\kappa)} \right\rangle A_{l_1 \dots l_f}, \quad (2.13a)$$

$$i \dot{\varphi}_m^{(\kappa)} = (1 - P^{(\kappa)}) \sum_{j,l=1}^{n_\kappa} \left[(\rho^{(\kappa)})^{-1} \right]_{mj} \langle H \rangle_{jl}^{(\kappa)} \varphi_l^{(\kappa)}. \quad (2.13b)$$

Here, the operator $P^{(\kappa)}$ refers to the projection onto the space spanned by the single-particle functions for the κ th degree of freedom,

$$P^{(\kappa)} = \sum_{j=1}^{n_\kappa} \left| \varphi_j^{(\kappa)} \right\rangle \left\langle \varphi_j^{(\kappa)} \right|, \quad (2.14)$$

and the mean-field Hamiltonian that is an operator acting on the κ th degree of freedom is defined as

$$\langle H \rangle_{jl}^{(\kappa)} = \langle \Psi | \varphi_j^{(\kappa)} \rangle H \langle \varphi_l^{(\kappa)} | \Psi \rangle. \quad (2.15)$$

The density matrix for the κ th degree of freedom, $\rho^{(\kappa)}$, is given by

$$\rho_{jl}^{(\kappa)} = \langle \Psi | \varphi_j^{(\kappa)} \rangle \langle \varphi_l^{(\kappa)} | \Psi \rangle. \quad (2.16)$$

$(\rho^{(\kappa)})^{-1}$ is the inverse matrix of $\rho^{(\kappa)}$.

Generally the employment of the MCTDH method allows us to treat the quantum dynamics of the system with tens of degrees of freedom.⁶⁷

3. ML-MCTDH

In the ML-MCTDH scheme,^{67–69} the SPF is replaced by a recursive layered expansion of the time-dependent basis function, which in nature is a way to decompose a high-dimensional tensor recursively into sums of several products of lower-dimensional tensors.⁸⁵ In principle, it is possible to combine a group of primary coordinates into a few logical coordinates (combined SPF bases). If the combined SPFs can be efficiently propagated, the calculation of the quantum evolution of the whole system becomes very efficient. However, if each combined SPF basis is the combination of too many primary coordinates, the computational efficiency may still be very low. In order to solve this problem, it is possible to split the combined modes again into even smaller groups of logical coordinates of the lower layer. Then, repeat this procedure over and over again until the primitive degrees of freedom are reached. This gives the recursive expansion of ML-MCTDH,

$$\begin{aligned} \varphi_m^{l-1; \kappa_1 \dots \kappa_{l-1}}(Q_{\kappa_{l-1}}^{l-1; \kappa_1 \dots \kappa_{l-2}}, t) \\ = \sum_{j_1=1}^{n_1} \cdots \sum_{j_{p_{\kappa_l}}=1}^{n_{\kappa_l}} A_{m; j_1 \dots j_{p_{\kappa_l}}}^{l; \kappa_1 \dots \kappa_{l-1}}(t) \prod_{\kappa_l=1}^{p_{\kappa_l}} \varphi_{j_{\kappa_l}}^{l; \kappa_1 \dots \kappa_l}(Q_{\kappa_l}^{l; \kappa_1 \dots \kappa_{l-1}}, t), \end{aligned} \quad (2.17)$$

where l denotes the layer depth, $\kappa_1, \dots, \kappa_{l-1}$ denote the indices of the logical degrees of freedom starting from the each node on the top layer and down to a particular primary

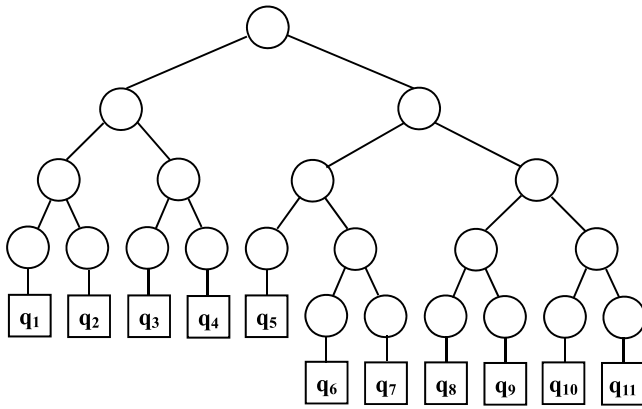


FIG. 1. Tree structure for the ML-MCTDH wavefunctions.

coordinate. Following this idea, a tree (or hierarchy) structure was constructed to represent the expansion of time-dependent basis over several layers (Fig. 1).

The EOMs of ML-MCTDH are similar to the usual MCTDH equations. For the top layer, they are identical to the MCTDH ones,

$$i \frac{\partial}{\partial t} A_J^1 = \sum_L \langle \Phi_J^1 | H | \Phi_L^1 \rangle A_L^1, \quad (2.18a)$$

$$\Phi_J^1 = \varphi_{j_1}^{(1;1)}(Q_1^1, t) \cdots \varphi_{j_p}^{(1;p)}(Q_p^1, t). \quad (2.18b)$$

The EOMs for the propagation of the SPFs are formally the same for all layers,

$$i \dot{\varphi}_n^{z, \kappa_l} = (1 - \hat{P}_{\kappa_l}^z) \sum (\rho_{nj}^{z, \kappa_l})^{-1} \langle H \rangle_{jm}^{z, \kappa_l} \varphi_m^{z, \kappa_l}, \quad (2.19)$$

where z is the shorted label for l ; $\kappa_1, \dots, \kappa_{l-1}$.

In practice, the recursive calculations of the mean-field Hamiltonians $\langle H \rangle^{(\kappa)}$ and the density matrices $\rho^{(\kappa)}$ are performed. As a promising way to perform the full quantum evolution of large systems, the initial test work has shown that it is possible to employ the ML-MCTDH method to treat the system with hundreds, even more than thousands degrees of freedom.⁶⁷

E. Initial condition

Within the Condon approximation, the initial wave packet $\Psi(t=0)$ is obtained by vertical excitation of the ground vibrational level of the electronic ground state to the donor state. The temperature effect on the current ET process is checked and proven to be very weak (shown in supplementary material⁸¹). Similar conclusions were made in previous experimental and theoretical studies.^{19,86} Thus, at the time zero, the nuclear wavefunction is assumed to be the ground vibrational level of the ground electronic state.

F. Electronic population probability

The diabatic population is defined as the expectation value of the projector $|\psi_\alpha\rangle\langle\psi_\alpha|$ with the time-dependent wave function,

$$P_\alpha(t) = \langle \Psi(t) | \psi_\alpha \rangle \langle \psi_\alpha | \Psi(t) \rangle, \quad (2.20)$$

where $|\psi_\alpha\rangle$ denotes the diabatic basis.

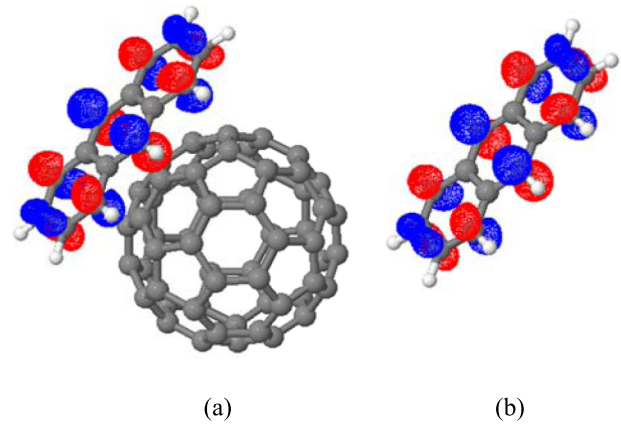


FIG. 2. (a) The selected LMO of the donor and (b) the LUMO of isolated anthracene.

III. RESULTS AND DISCUSSION

A. Donor and acceptor states selection

We choose the donor LMO that resembles to the LUMO of the isolated anthracene as the donor state, whose MO profile is shown in Fig. 2. This selection should be reasonable since the first excited state of anthracene corresponds to the HOMO \rightarrow LUMO transition.

In order to choose the acceptor states with important contribution to the ET process, 14 unoccupied LMOs of C60 (energetically close to the donor state) are firstly chosen as the acceptor states to study the pure electronic dynamics without the inclusion of the nuclear degrees of freedom. As shown in Fig. 3, three unoccupied acceptor states, denoted as A1, A2, A3, are responsible for the ET process, and their MO profiles are given in Fig. 4. Such multiple-acceptor-state feature is caused by the existence of three nearly degenerated virtual orbitals due to the high symmetry of C₆₀. The contributions of other acceptor states can be neglected, because their populations remain nearly zero during the quantum evolution. Thus, it is enough to employ a four-state model with one donor state (D) and three

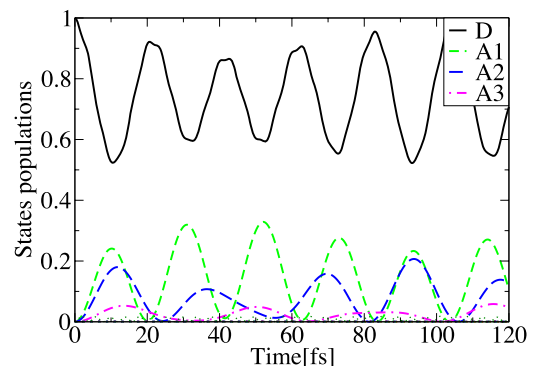


FIG. 3. Quantum evolution of the pure electronic dynamics based on the model Hamiltonian including the single donor state and 14 acceptor states. The upper line (D) denotes the population of the donor state and the other lines denote the populations of acceptor states. Three acceptor states are mainly responsible for the ET process, denoted as A1, A2, A3. The other 11 acceptor states give very little contribution because their populations remain nearly zero during the dynamics evolution.

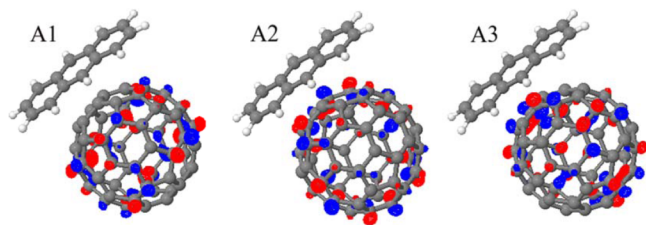


FIG. 4. Three selected localized acceptor states.

acceptor states (A1, A2, A3) in the full quantum dynamics calculations including vibrational motion. The parameters in the diabatic Hamiltonian, i.e., the energies of the donor and acceptor states, as well as the donor-acceptor coupling matrix elements, are given in the Appendix.

B. Vibronic couplings

The vibrational frequencies ω_i and the corresponding vibronic coupling constants $\kappa_i^{d/a}$ of the donor and acceptor states were determined for all 246 vibrational modes of the anthracene/C60 complex, as described in Sec. II. The shift of potential minimum, Δx_i , along each mode is

$$\Delta x_i = \frac{\kappa_i^a - \kappa_i^d}{\omega_i}, \quad (3.1)$$

which reflects the vibronic contribution of each mode on the ET process. The dependences of Δx_i on the vibrational frequencies are shown in Fig. 5, which can be viewed as one of the criteria to select the important modes in the quantum dynamics simulation. In addition, the vibrational modes in resonance with the Rabi oscillation of the pure electronic dynamics should also play important role.

Although the low-frequency intermolecular vibrations with $\omega_i < 100 \text{ cm}^{-1}$ show large Δx_i , they play rather minor roles in the quantum dynamics simulation of the ET process (see below discussions). Thus, we also show the Δx_i values

for all intramolecular vibrational modes ($\omega_i > 100 \text{ cm}^{-1}$) in the right side of Fig. 5. The low-frequency modes ($< 100 \text{ cm}^{-1}$) correspond to the intermolecular motions, and the high-frequency modes ($> 3000 \text{ cm}^{-1}$) correspond to the CH stretching motion. The deformations of these modes are given in the supplementary material.⁸¹

According to the vibronic couplings of all vibrational modes, three groups of modes with pronounced coupling strengths are easily recognized in different energy domains. If we treat all nuclear vibrational motions as the bath of harmonic oscillators, the spectral density can be built based on the vibronic couplings of all modes.⁸⁷ Then, it is easy to conclude that the overall spectral density should contain three main peaks at around 0.005 eV, 0.05 eV, and 0.18 eV, respectively. Thus, in principle, it is possible to use three harmonic-oscillator baths with different character frequencies ($\omega_c \sim 0.005, 0.05$, and 0.18 eV) to represent all vibrational modes. In previous work by Tamura *et al.*,²⁰ they also locate the similar two peaks around 0.06 eV and 0.2 eV in the spectral density for the similar system. In our work, the intermolecular motions are included as well, thus the current spectral density contains the contribution from the low-frequency (0.005 eV) domain.

Taking the two-level system (D and A1) as an example, the electronic coupling $\Delta = 0.05 \text{ eV}$ (V_{DA1}). The ultrafast ET dynamics is not influenced by the low-frequency modes (see below discussion), thus their roles are not concerned here. When the bath includes all vibrational modes within the second frequency region ($\omega_c \sim 0.05 \text{ eV}$), the parameter Δ/ω_c is close to 1. If we consider the bath composed of modes within the third frequency domain ($\omega_c \sim 0.18 \text{ eV}$), the parameter Δ/ω_c is around to 0.25. Thus, the current ET dynamics falls into the intermediate to nonadiabatic ET region. In addition, the vibronic couplings strength is rather high compared with the pure electronic couplings. The diabatic energy difference between the donor and acceptor states is also larger than the electronic coupling. Previous theoretical studies⁸⁷ once pointed out that it is not possible

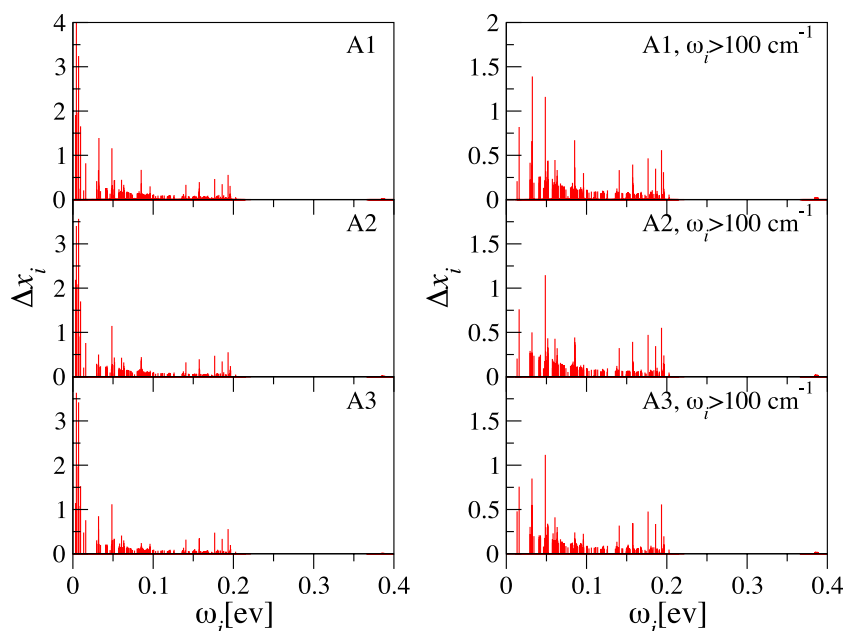


FIG. 5. The shift of potential minima, Δx_i , for all normal modes (left column) and along the modes with $\omega_i > 100 \text{ cm}^{-1}$ (right column) for the three acceptor states (denoted as A1, A2, A3).

to use approximated methods, such as the Redfield equation, to treat the ET dynamics in the case of intermediate to nonadiabatic ET region, strong system-bath (vibronic) couplings, and the significant diabatic D-A energy difference with respect to their coupling. In addition, the group of modes with frequency close to 0.18 eV is resonance with the Rabi oscillation of pure electronic dynamics. The similar time scale of electronic dynamics and these vibrational motions indicates that the current ET dynamics is essentially non-Markovian, thus it is highly preferred to employ the ML-MCTDH method to obtain the precise theoretical treatment.

C. ET dynamics

In this section, we first investigated the quantum evolution of the 2S models only including the donor and A1 states. Two criteria are considered to determine which modes are important to the ET dynamics. The first criterion is the shift of potential minimum, Δx_i , along each mode. In addition, the vibrational modes in resonance with the Rabi oscillation of the pure electronic dynamics should also be largely concerned.

In order to characterize the influence of modes with different Δx_i on quantum evolution, a series of quantum dynamics calculations were performed. First, the ET dynamics only considering two modes with largest coupling strengths were simulated by using our home-made quantum-dynamics program, MCTDH, and ML-MCTDH for comparison. Here, the two modes, i.e., ν_{15} and ν_{26} , were selected, because they display the largest vibronic couplings and do not belong to low-frequency intermolecular vibrations. Their deformations are displayed in the supplementary material.⁸¹ The same results are obtained from all dynamics methods (data given in the supplementary material),⁸¹ which means that we successfully get precise results by using MCTDH and ML-MCTDH for reduced systems. Next, the high-dimensional ET dynamics with many vibrational degrees of freedom were investigated by MCTDH and ML-MCTDH. When the number of vibrational modes is small, MCTDH can give identical results as ML-MCTDH. For example, the same results were obtained in the case that all 11 modes with $\Delta x_i > 0.5$ are included (see the supplementary material).⁸¹ With the increasing of the degrees of freedom, the convergence of the standard MCTDH calculations becomes very difficult to be achieved due to the large number of basis functions (shown in the supplementary material).⁸¹ Thus in this case, only the ML-MCTDH results are considered in discussions.

Fig. 6 shows the population decay of the photo-generated donor state when different number of vibrational modes is included. In the pure electronic dynamics without the inclusion of nuclear degrees of freedom, the population of the donor state exhibits pronounced oscillatory features corresponding to electronic coherence (the curve A in Fig. 6). When the nuclear motion is involved, the vibronic couplings immediately lead to a significant damping effect on electronic motions. Even when only two important modes are introduced, the oscillation feature becomes weaker obviously (the curve B in Fig. 6). With the increasing of more vibrational modes, the oscillation is largely suppressed and the

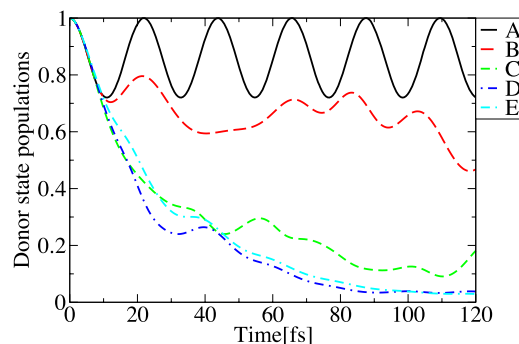


FIG. 6. The populations of the donor state with the model including zero modes (A), two modes ν_{15} and ν_{26} (B), 11 modes ($\Delta x_i > 0.5$) (C), 44 modes ($\Delta x_i > 0.2$) (D), and all 246 modes (E).

population recurrence becomes less pronounced. When 11 modes ($\Delta x_i > 0.5$) are included, the population of the donor state decays rather rapidly and the oscillation becomes very weak (the curve C in Fig. 6). When even more vibrational modes (44 modes with $\Delta x_i > 0.2$) are included, only one recurrent peak appears at about 40 fs. Finally, when all 246 modes are involved, the large number of vibrations results in the strong damping effect on the electronic coherence, resulting in the significant quenching of the recurrences in the electronic-population dynamics. The further discussion on the coherent transfer dynamics is given in the Appendix. Nevertheless, the inclusion of vibrational modes with $\Delta x_i < 0.2$ still gives the visible impact on the population dynamics, thus it is necessary to employ the full-dimensional model with all vibrational degrees of freedom to achieve the precise understanding of the ET process in complex systems.

The four adiabatic energies and the expected Rabi frequencies for the three main D \rightarrow A transitions are given in the Appendix. These data allow us to determine the spectral domain where the vibrational modes are expected to be in resonance with the pure electronic transition. Particularly, the modes with frequencies close to the Rabi frequency should be paid attention. To check the influence of these modes on the ET dynamics, several diabatic 2S models (D and A1) were built, which include vibrational modes within the different ranges of frequency domains centered at the Rabi frequency (~ 0.190 eV). Next, we label the pure electronic dynamics as Case A and other nonadiabatic dynamics as Case B-E (Fig. 7).

Case B considers the frequency domain of 0.190 ± 0.003 eV (1508.29 – 1556.69 cm^{-1}), in which the coupling strengths Δx_i of these modes are all smaller than 0.1. When these modes are included, the early stage ET dynamics (Case B) is very similar to the pure electronic dynamics (Case A) [Fig. 7]. After a few Rabi-oscillation cycles, the overall donor population in Case B starts to decay obviously and this implies the energy transfer from electronic motion to the nuclear motion, while the oscillation pattern and its period remain almost unchanged. When a little larger frequency domain 0.190 ± 0.004 eV (1500.23 – 1564.75 cm^{-1}) is considered in the Case C, two modes ν_{223} (1559.49 cm^{-1} , $\Delta x_i = 0.56$) and ν_{214} (1500.22 cm^{-1} , $\Delta x_i = 0.35$) with strong visible couplings are included in the 2S model. The inclusion of

states) with all 246 modes. Compared to the 2S models, the population of the donor state decays faster (~ 16 fs), while the populations of the acceptor states quickly reach to the plateau, see Fig. 9(a). The A1 state gives the primary contribution ($\sim 60\%$) in the ET dynamics, while both A2 ($\sim 30\%$) and A3 ($\sim 10\%$) also play important roles here. Thus consistent with previous discussions, all three acceptor states should be involved in the ET processes.

It is worthwhile to check the contribution of the low-frequency intermolecular modes ($\omega_i < 100\text{ cm}^{-1}$) on the ET dynamics, since they are not well described by the harmonic oscillator approximation. In addition, the electronic-structure calculations show that they have large vibronic coupling strengths (Fig. 5). However, the removal of all low-frequency modes does not change the ET dynamics at all, see Fig. 9(b). Thus, the low-frequency intermolecular vibrational modes should play minor roles here. The reason is very obvious. It should be possible to separate the slow low-frequency motions and current ultrafast ET dynamics due to their different time scales. Thus, it should be safe to neglect these low-frequency modes in the treatment of ultrafast ET dynamics for complex systems. Alternatively, it is also acceptable to employ the harmonic oscillator approximation for the low-frequency modes in the construction of the full-dimensional Hamiltonian model, because they give very minor contributions. As shown in Fig. 9(c), when the modes with high frequencies related to the C—H stretching vibration are removed, the dynamics is very similar to the results with the full-dimensional model. The reasons seem to be obvious. They are neither the strong coupling modes nor the modes with resonance with the Rabi oscillation. Thus, in principle, these modes are also not important in the current ET dynamics.

To examine the dependence of the ET dynamics on the electronic-structure levels, we also try to run the ML-MCTDH dynamics with the model built from other functionals (B3LYP and LC- ω PBE). The diabatic Hamiltonian was re-constructed by replacing the zero order terms (V_{dd} , V_{aa} , and V_{da} in Eqs. (2.2) and (2.3)) by their corresponding values obtained with these hybrid functionals (the supplementary material).⁸¹ The ET dynamics based on these new diabatic models are given in the supplementary material.⁸¹ In the current system, the ET dynamics does not change dramatically when the different electronic-structure levels are employed.

The photo-induced ET process is critical for the solar energy conversion in OSCs. As discussed previously, different theoretical approaches were taken by several groups, ranging from surface-hopping dynamics,⁴⁰ real-time TDDFT,⁴³ and standard MCTDH.^{18–20} However, all of these methods suffer from various deficiencies. Thus, the employment of novel quantum dynamics method to understand the ET process of complex systems with very high dimensionality is very essential. As the powerful extension of the standard MCTDH method, ML-MCTDH gives us the possibility to understand the ET processes involving huge number of degrees of freedom with high efficiency and accuracy. The results derived from ML-MCTDH calculations can also be the “benchmark” to examine the validation of other approximated dynamics methods. In this sense, it is very essential

to employ such powerful methods to study photo-induced electron transfers or energy transfers in OSCs. For example, in this work, we have successfully simulated the quantum dynamics of the ET process involving 4 electronic states and all 246 nuclear degrees of freedom within the ML-MCTDH framework. In addition, some important views may be obtained from such calculations. For example, more than one acceptor states should be included to achieve the reasonable description of the ET process. This highly indicates that it may not be enough to only consider a single acceptor states when dealing with the ET process in complex systems such as OSCs, which was indicated by Burghardt and coworkers as well.⁶³

Previous study pointed out that the formalism of ML-MCTDH is relevant to the tensor decomposition. A high-order tensor can be decomposed recursively into sums of products of low-dimensional tensors by the so-called “hierarchical Tucker form” represented by a tree structure.⁸⁵ This tree-type Tucker form in principle may significantly reduce the computational cost in the solution of the high-dimensional differential equations. However, such hierarchical Tucker form is not uniquely defined, implying different tree structures may be constructed for the same ML-MCTDH calculation. The construction of the reasonable tree structure is not a trivial task,^{67–69} since the EOMs for all layers should be solved to achieve converged results. The less nodes in each layer result in the smaller effective Hamiltonian (Eq. (2.15)) matrices, largely reducing the computational cost for the solution of the corresponding EOMs. However, in this case, more EOMs should be solved due to the increasing of the layer number in the ML-MCTDH expansion.

Although previous works did not explicitly give the step-by-step tutorial for the construction of the ML-MCTDH tree, some useful comments were discussed.^{67–69} The similar principle was used in the ML-MCTDH tree construction by considering below issues. (1) The top layer is composed of two nodes, the electronic degree of freedom and the nuclear degrees of freedom. (2) The vibrational modes are separated into two groups: system ($\Delta x_i > 0.2$) and bath ($\Delta x_i < 0.2$). (3) In the system group, the modes with similar Δx_i are put together to build a few sub-groups (nodes). (4) For the bath part, the much smaller size of basis functions should be used and we group them by frequency. According to these rules, an initial tree is built. The ML-MCTDH calculation with a set of relatively small-sized basis functions was performed for test purpose. Then, the branched-structure of tree is re-arranged based on the node populations. Particularly, the strong coupled modes should be put together in the construction of a new ML-MCTDH tree. Following this process iteratively, a reasonable tree can be constructed after several test runs. In the current work, some test calculations were first performed based on different trees with 2, 3, 4, and 5 branches for the top layer and different setups of other layers. Then, we always found that the trees with more 2-branched layers seem to give faster computation for the current system. Thus, we finally took 2 branches for each layer and the computational cost looks reasonable after additional test calculations for convergence. For the largest ML-MCTDH calculations in the current work, the nine-layer tree was

used to treat the full-dimensional model including 4 states and all vibrational modes. In fact, this special hierarchical Tucker form corresponds to the so-called “dimension tree.”⁸⁵ Certainly, the current ML-MCTDH calculations in fact do not involve the extremely large number of vibrational modes that give large contributions on the ET dynamics. It is not sure that the dimensional tree displaying reasonable efficiency in the current work also fits well for other situations. The optimal construction of hierarchical tree structures for the efficient and accurate treatment of more complex systems with high dimensionality remains the great challenging for the future studies.

As discussed before, the ML-MCTDH is a very powerful method in the exact treatment of the quantum dynamics of complex systems. However, the description of extremely large systems may result in a huge hierarchical tree even beyond the treatable limit of the ML-MCTDH. The combination of the effective-mode approach^{20,71,88} and the ML-MCTDH method may give a possible solution for this challenge.

IV. CONCLUSIONS AND OUTLOOKS

In this paper, we wish to describe the quantum dynamics of the ET process between anthracene and C60. The diabatic Hamiltonian is built, which includes one electronic donor and several acceptor states, localized at anthracene and C60, respectively. In the model construction, the An/C60 complex is separated into two parts (a donor part and an acceptor part), and a subsequent diagonalization of the two blocks of the electronic Hamiltonian is employed to construct the donor and acceptor states. Within the framework of single-electron picture, the Fock matrix in the Löwdin orthogonal AO bases is divided into four blocks, and two diagonal ones represent the electronic Hamiltonian for donor and acceptor, respectively. The diagonalization of two blocks finally gives us the localized states (orbitals) and their couplings. The full dimensional quantum dynamics of the ET process were simulated using the ML-MCTDH method with a nine-layer dimension tree, which allows an efficient and accurate description of this system comprising 4 electronic states and all the 246 nuclear degrees of freedom. The results demonstrate the existence of an ultrafast ET process in this system. Here, three (not one) acceptor states play key roles in the ET process. The ET dynamics without nuclear motion exhibits significant electronic coherence effects. The inclusion of the nuclear degrees of freedom results in the strong quenching of coherence effects. The low-frequency vibrational modes that are corresponding to intermolecular ones have very little contribution to the ET dynamics.

The current calculations show that the ML-MCTDH method up to the infinity number of layers is a very powerful tool, which can deal with the quantum dynamics involving the huge number of degrees of freedom. Thus, the ML-MCTDH method is very suitable to study the nonadiabatic processes in complex systems. Although there is no direct experimental observation on the current An-C60 system, many experimental works confirmed the existence of the ultrafast excitation energy transfer and ET dynamics

(<100 fs) in other OPV systems.^{2,5-17} Thus, it should be very interesting to use ML-MCTDH to study these ultrafast dynamics in these realistic organic photovoltaic (OPV) systems.

As our first efforts to understand the ET process in OSCs, the current model is still rather approximated. For example, our diabatic Hamiltonian model is based on a preliminary approximation within the single-electron picture and does not explicitly treat the excited electronic states. It is challenging to improve the way to construct the diabatic Hamiltonian by more accurate models. In last few years, several theoretical approaches were proposed to build such diabatic Hamiltonian, such as variants of the generalized Mulliken-Hush and coulomb coupling schemes by Hsu,⁸⁹⁻⁹² Köhn,⁹³ and their co-workers, localized diabatization algorithms by Subotnik and co-workers,^{94,95} multistate density functional theory by Gao and co-workers.²⁷ With the development of these schemes, it should be possible to run ML-MCTDH based on the more accurate diabatic model with several electronic states and many vibrational degrees of freedom. In addition, the current work only takes two stacked molecules to build a simplified model. In reality, different stacked statuses of BHJ may appear in OSCs, it should also be interesting to consider this effect in the simulation of real systems. All of above topics will be the subjects of our future work.

ACKNOWLEDGMENTS

This work is supported by CAS 100 talent project and NSFC projects (Nos. 21103213 and 91233106), Key Lab of Nanodevices and Nanoapplications, CAS (Grant No. 14HZ03), and the Director Innovation Foundation of CAS-QIBEBT. The authors thank the Supercomputing Center, Computer Network Information Center, CAS, National Supercomputing Center in Shenzhen, and the Supercomputational Center of CAS-QIBEBT for providing computational resources.

APPENDIX: COMPUTATIONAL DETAILS AND COHERENT TRANSFER DYNAMICS

1. Parameters

The parameters (zeroth-order terms without vibronic coupling) in the diabatic Hamiltonian and the corresponding Rabi frequencies are given in Tables I and II.

TABLE I. The energies of the diabatic and adiabatic states.

States	1	2	3	4
$V_{ii,adia}$ (eV)	-2.949	-2.905	-2.875	-2.745
$V_{ii,dia}$ (eV)	-2.762	-2.922	-2.889	-2.864

TABLE II. The donor-acceptor coupling elements and the Rabi frequencies.

	A1	A2	A3
V_{da} (eV)	0.050	0.038	-0.018
ω (eV)	0.190	0.148	0.096

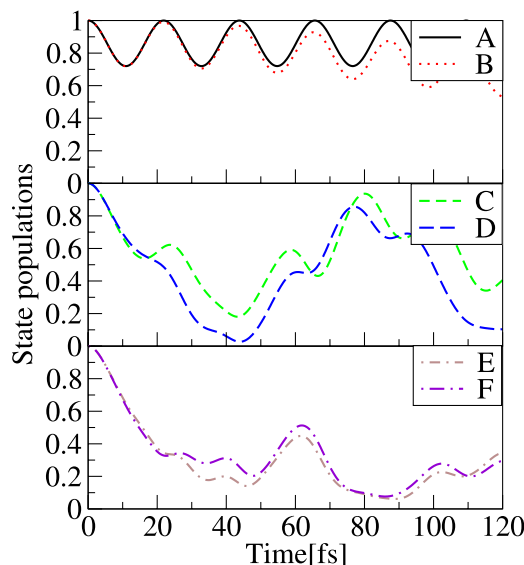


FIG. 7. The populations of the donor state in the 2S model (D and A1) without any vibrational modes (A) and with the vibrational modes within different frequency ranges centered at Rabi frequency (0.190 eV): B. 1508.29–1556.69 cm^{-1} (0.190 ± 0.003 eV), C. 1500.23–1564.75 cm^{-1} (0.190 ± 0.004 eV), D. 1451.83–1613.15 cm^{-1} (0.190 ± 0.01 eV), E. 1129.20–1935.78 cm^{-1} (0.190 ± 0.05 eV), F. 1129.20–1935.78 cm^{-1} (0.190 ± 0.05 eV, $\Delta x_i > 0.2$).

such mode immediately changes the ET dynamics completely (Fig. 7). The significant ET takes place and the population of the donor state drops below 0.1 within 40–50 fs, while the strong recurrence and large-amplitude oscillation patterns appear afterwards. When the frequency domain becomes larger (Case D: 0.190 ± 0.01 eV, 1451.83–1613.15 cm^{-1}), the ET dynamics does not significantly change from Case C to D, possible because only one additional mode ν_{230} (1579.47 cm^{-1} , $\Delta x_i = 0.31$) with large Δx_i is included. When the domain with very broad frequency range (Case E: 0.190 ± 0.05 eV, 1129.20–1935.78 cm^{-1}) is considered, the initial fast drop of donor-state population is observed, while the recurrence is largely suppressed. This highly implies that the inclusion of more vibrational modes induces the effective damping effects and suppresses the recurrence significantly. Similar dynamics behaviors are obtained when we only take all modes with $\Delta x_i > 0.2$ within the same frequency domain of Case E; see the result of Case F.

Overall, two important criteria should be taken into account to determine which mode plays dominant role in the ultrafast ET dynamics, namely, the modes with the large vibronic couplings and the frequency close to the Rabi frequency. If a mode satisfies both criteria, it becomes very important for the ultrafast ET dynamics.

When the propagation time duration increases up to 1 ps, the diabatic population keeps the asymptotic equilibrium value and no recurrence occurs (shown in the supplementary material).⁸¹ According to previous studies,²⁰ it is possible to define the Poincaré recurrence period $\tau_p = 2\pi/\Delta\omega$ based on the frequency interval $\Delta\omega$ between two adjacent modes. As shown in the supplementary material,⁸¹ the frequency difference between two adjacent modes may be smaller than 10 cm^{-1} (shown in the supplementary material⁸¹). Thus, the

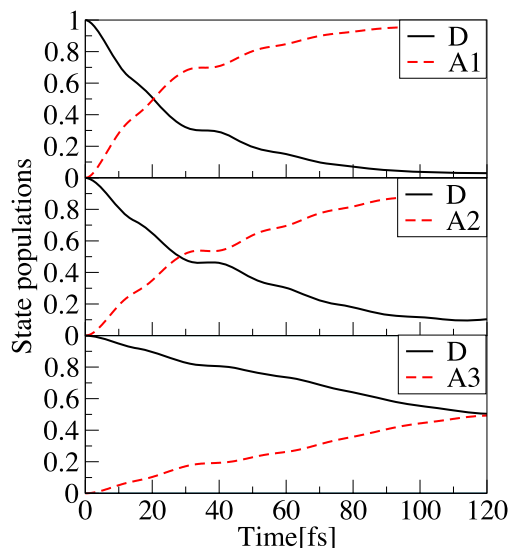


FIG. 8. The populations of the donor and acceptor states in the reduced models with two states and all vibrational modes.

Poincaré recurrence period τ_p is longer than 3 ps, which is far beyond the time scale of the current ET dynamics. This is consistent to the fact that no recurrence occurs within the 1 ps time duration (see the supplementary material).⁸¹

Quantum dynamic calculations of three 2S models (only including the donor state and different acceptor states, all 246 modes) were performed using ML-MCTDH (shown in Fig. 8). The simulation predicts an ultrafast injection of the electron from the donor state localized at the anthracene into one of the three acceptor states (A1, A2, and A3) localized at the C60 on a time scale of about 20, 28, and 120 fs, respectively. Thus, in principle, all three acceptor states should be taken into account for the completed description of the ET process in OSC systems.

Furthermore, the full dimensional quantum dynamic simulation was performed using ML-MCTDH, based on the 4S model (including the donor state and the three acceptor

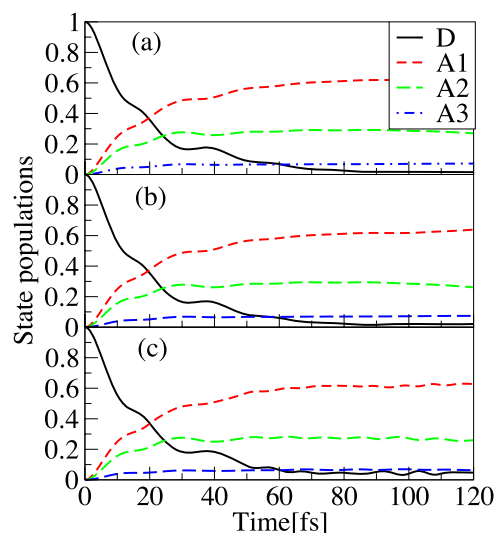


FIG. 9. The populations of the donor state and the three acceptor states in the 4S model with all vibrational modes (a), with modes whose frequency $\omega_i > 100$ cm^{-1} (b), and with modes whose frequency $\omega_i < 3000$ cm^{-1} (c).

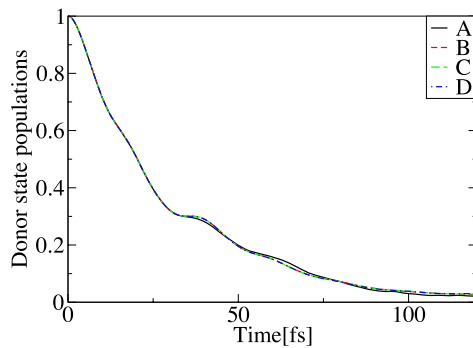


FIG. 10. The populations of the donor state in the 2S model (D-A1) with different convergences. For the four ML-MCTDH calculations, the smallest NPs of the two logical coordinates at the top layer are (A. $5.9 \times 10^{-3}/5.1 \times 10^{-3}$), (B. $1.8 \times 10^{-4}/1.0 \times 10^{-4}$), (C. $5.3 \times 10^{-5}/2.0 \times 10^{-5}$), and (D. $9 \times 10^{-6}/4 \times 10^{-6}$), respectively.

TABLE III. Total CPU times (t_{ML}) of ML-MCTDH calculations (Fig. 10) with different convergences (characterized by the smallest NPs of the two logical coordinates at the top layer).

NPs	t_{ML} (h:m)
$5.9 \times 10^{-3}/5.1 \times 10^{-3}$	8:49
$1.8 \times 10^{-4}/1.0 \times 10^{-4}$	42:54
$5.3 \times 10^{-5}/2.0 \times 10^{-5}$	78:59
$9 \times 10^{-6}/4 \times 10^{-6}$	379:58

TABLE IV. Total CPU times of MCTDH and ML-MCTDH calculations including different modes with convergences at 10^{-5} level corresponding to Fig. 7. N_{modes} denotes the number of modes involved in calculations, and t_{MCTDH} and t_{ML} denote the CPU times of MCTDH and ML-MCTDH calculations, respectively.

N_{modes}	t_{MCTDH} (h:m:s)	t_{ML} (h:m:s)
2	0:0:5	0:0:6
11	155:46:52	0:27:26
44	...	8:29:57
246	...	78:59

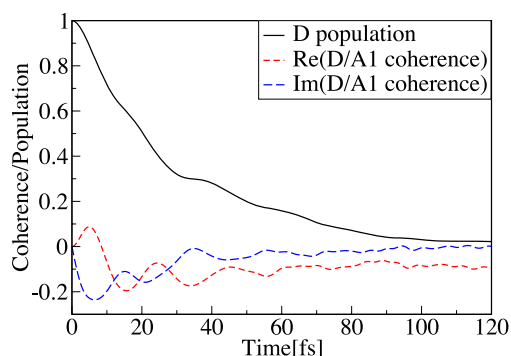


FIG. 11. Time-evolving electronic coherence and the population transfer in the 2S model (D-A1) with all vibrational modes.

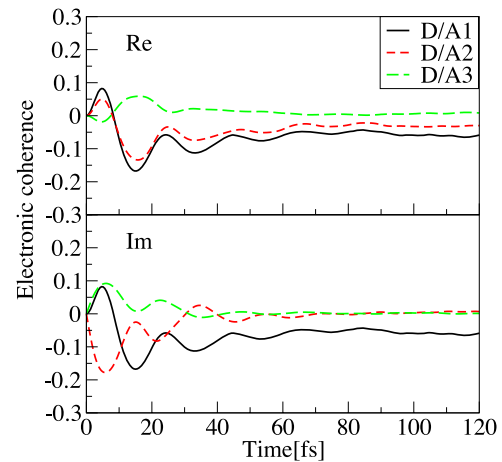


FIG. 12. Time-evolving electronic coherence in the 4S model with all vibrational modes.

2. Convergence check

The convergences of ML-MCTDH calculations were checked and the results are shown in Fig. 10. The eigenvalues of the density matrices (defined in Eq. (2.18)) at each layer, namely, the natural populations (NPs), provide one of indications for the convergence of a ML-MCTDH calculation.⁶⁷

3. Propagation time

The total CPU times of the calculations by using MCTDH and ML-MCTDH methods with different convergences are listed in Tables III and IV. All the listed calculations in these two tables are run on the machine with the single CPU [Intel(R) Xeon(R) Processor (E3-1220 V2 and 3.10 GHz)].

4. Coherent transfer dynamics

When all vibrational modes are included in the 2S model (D-A1), the donor-state population decays almost monotonically. However, some plateaus still seem to exist in the decay of the donor-state population (Fig. 11), which indicates the very weak recurrence in the ET dynamics. To further analyze this question, the time-dependent electronic coherence is measured by the off-diagonal elements $\bar{\rho}_{A,D}(t)$ of the reduced electronic density matrix,

$$\bar{\rho}_{A,D}(t) = \text{Tr} \{ |\psi_D\rangle \langle \psi_A| \hat{\rho}(t) \} = \int \rho_{A,D}(Q,t) dQ, \quad (A1)$$

where the density operator is given by ($\hat{\rho}(t) = |\Psi(t)\rangle \langle \Psi(t)|$) and the trace (Tr) is over all vibrational degrees of freedom.^{20,21} As shown in Fig. 11, both the real part and imaginary part of $\bar{\rho}_{A,D}(t)$ display the obvious oscillation patterns in the early state of the ET dynamics, whose periods are consistent with the appearance of the plateaus in the donor-state population decay. This indicates that the weak recurrence feature is in accordance with the D/A1 electronic coherence. The electronic coherence vanishes very fast (~ 80 fs) when the donor-state population reaches a stable value. After it, the imaginary term of $\bar{\rho}_{A,D}(t)$ decays completely to zero, while the real part of

$\bar{\rho}_{A,D}(t)$ becomes a small constant value. Similar findings are also observed in the 4S model with all vibrational modes (Fig. 12). In fact, the existence of the significant electronic coherence in the early stage of the ET dynamics was noticed by previous work.^{20,21}

- ¹N. S. Lewis, *Science* **315**, 798 (2007).
- ²A. J. Heeger, *Adv. Mater.* **26**, 10 (2014).
- ³C. W. Lee, O. Y. Kim, and J. Y. Lee, *J. Ind. Eng. Chem.* **20**, 1198 (2014).
- ⁴A. Uddin and X. H. Yang, *J. Nanosci. Nanotechnol.* **14**, 5752 (2014).
- ⁵L. G. Kaake, G. C. Welch, D. Moses, G. C. Bazan, and A. J. Heeger, *J. Phys. Chem. Lett.* **3**, 1253 (2012).
- ⁶L. G. Kaake, D. Moses, and A. J. Heeger, *J. Phys. Chem. Lett.* **4**, 2264 (2013).
- ⁷Y. Huang, F. Liu, X. Guo, W. Zhang, Y. Gu, J. P. Zhang, C. C. Han, T. P. Russell, and J. H. Hou, *Adv. Energy Mater.* **3**, 930 (2013).
- ⁸R. D. Pensack, C. H. Guo, K. Vakhshouri, E. D. Gomez, and J. B. Asbury, *J. Phys. Chem. C* **116**, 4824 (2012).
- ⁹K. S. Jeong, R. D. Pensack, and J. B. Asbury, *Acc. Chem. Res.* **46**, 1538 (2013).
- ¹⁰A. Rao, P. C. Y. Chow, S. Gelinas, C. W. Schlenker, C.-Z. Li, H.-L. Yip, A. K. Y. Jen, D. S. Ginger, and R. H. Friend, *Nature* **500**, 435 (2013).
- ¹¹B. Bernardo, D. Cheyns, B. Verreest, R. D. Schaller, B. P. Rand, and N. C. Giebink, *Nat. Commun.* **5**, 3245 (2014).
- ¹²B.-C. Lin, B. T. Koo, P. Clancy, and C.-P. Hsu, *J. Phys. Chem. C* **118**, 23605 (2014).
- ¹³H. B. Wang and M. Thoss, *J. Chem. Phys.* **119**, 1289 (2003).
- ¹⁴I. Kondov, M. Čížek, C. Benesch, H. B. Wang, and M. Thoss, *J. Phys. Chem. C* **111**, 11970 (2007).
- ¹⁵J. Li, I. Kondov, H. Wang, and M. Thoss, *J. Phys. Chem. C* **114**, 18481 (2010).
- ¹⁶J. Li, H. Wang, P. Persson, and M. Thoss, *J. Chem. Phys.* **137**, 22A529 (2012).
- ¹⁷M. Thoss, I. Kondov, and H. B. Wang, *Phys. Rev. B* **76**, 153313 (2007).
- ¹⁸I. Burghardt, E. Bittner, H. Tamura, A. Pereverzev, and J. Ramon, in *Energy Transfer Dynamics in Biomaterial Systems*, edited by I. Burghardt *et al.* (Springer, Berlin, Heidelberg, 2009), p. 183.
- ¹⁹H. Tamura, I. Burghardt, and M. Tsukada, *J. Phys. Chem. C* **115**, 10205 (2011).
- ²⁰H. Tamura, R. Martinazzo, M. Ruckebauer, and I. Burghardt, *J. Chem. Phys.* **137**, 22A540 (2012).
- ²¹A. Chenel, E. Mangaud, I. Burghardt, C. Meier, and M. Desouter-Lecomte, *J. Chem. Phys.* **140**, 044104 (2014).
- ²²K. H. Hughes, B. Cahier, R. Martinazzo, H. Tamura, and I. Burghardt, *Chem. Phys.* **442**, 111 (2014).
- ²³T. Wang, G. Brudvig, and V. S. Batista, *J. Chem. Theory Comput.* **6**, 755 (2010).
- ²⁴L. Wang, Q. Li, Z. Shuai, L. Chen, and Q. Shi, *Phys. Chem. Chem. Phys.* **12**, 3309 (2010).
- ²⁵J. Ren, S. Meng, and E. Kaxiras, *Nano Res.* **5**, 248 (2012).
- ²⁶Y. Yi, V. Coropceanu, and J.-L. Bredas, *J. Am. Chem. Soc.* **131**, 15777 (2009).
- ²⁷W. L. Chan, T. C. Berkelbach, M. R. Provorse, N. R. Monahan, J. R. Tritsch, M. S. Hybertsen, D. R. Reichman, J. L. Gao, and X. Y. Zhu, *Acc. Chem. Res.* **46**, 1321 (2013).
- ²⁸O. Kühn and S. Lochbrunner, *Semicond. Semimetals* **85**, 47 (2011).
- ²⁹A. Neubauer, G. Grell, A. Friedrich, S. I. Bokarev, P. Schwarzbach, F. Gartner, A. E. Surkus, H. Junge, M. Beller, O. Kühn, and S. Lochbrunner, *J. Phys. Chem. Lett.* **5**, 1355 (2014).
- ³⁰L. G. C. Rego and V. S. Batista, *J. Am. Chem. Soc.* **125**, 7989 (2003).
- ³¹H. Ma and A. Troisi, *Adv. Mater.* **26**, 6163 (2014).
- ³²L. Han, X. Zhong, W. Liang, and Y. Zhao, *J. Chem. Phys.* **140**, 214107 (2014).
- ³³X. Zhong and Y. Zhao, *J. Chem. Phys.* **138**, 014111 (2013).
- ³⁴F. Gao, Y. Zhao, and W. Liang, *J. Phys. Chem. B* **115**, 2699 (2011).
- ³⁵S. G. Abuabara, L. G. C. Rego, and V. S. Batista, *J. Am. Chem. Soc.* **127**, 18234 (2005).
- ³⁶T. C. Berkelbach, M. S. Hybertsen, and D. R. Reichman, *J. Chem. Phys.* **141**, 074705 (2014).
- ³⁷F. Ding, E. B. Guidez, C. M. Aikens, and X. Li, *J. Chem. Phys.* **140**, 244705 (2014).
- ³⁸G. Tao, *J. Phys. Chem. C* **118**, 17299 (2014).
- ³⁹W. Stier and O. V. Prezhdo, *J. Phys. Chem. B* **106**, 8047 (2002).
- ⁴⁰A. V. Akimov and O. V. Prezhdo, *J. Am. Chem. Soc.* **136**, 1599 (2014).
- ⁴¹A. V. Akimov, A. J. Neukirch, and O. V. Prezhdo, *Chem. Rev.* **113**, 4496 (2013).
- ⁴²W. Stier, W. R. Duncan, and O. V. Prezhdo, *Adv. Mater.* **16**, 240 (2004).
- ⁴³S. M. Falke, C. A. Rozzi, D. Brida, M. Maiuri, M. Amato, E. Sommer, A. De Sio, A. Rubio, G. Cerullo, E. Molinari, and C. Lienau, *Science* **344**, 1001 (2014).
- ⁴⁴V. May and O. Kühn, *Charge and Energy Transfer Dynamics in Molecular Systems*, 3rd ed. (WILEY-VCH Verlag GmbH & Co., KGaA, Germany, 2011).
- ⁴⁵Y. Tanimura and R. Kubo, *J. Phys. Soc. Jpn.* **58**, 101 (1989).
- ⁴⁶Y. Tanimura, *J. Phys. Soc. Jpn.* **75**, 082001 (2006).
- ⁴⁷J. Xu, R. X. Xu, M. Luo, and Y. J. Yan, *Chem. Phys.* **370**, 109 (2010).
- ⁴⁸G.-J. Nan, R.-H. Zheng, Q. Shi, and Z.-G. Shuai, *Acta Phys.-Chim. Sin.* **26**, 1755 (2010).
- ⁴⁹F. A. Shakib and G. Hanna, *J. Chem. Phys.* **141**, 044122 (2014).
- ⁵⁰L. G. C. Rego, S. G. Abuabara, and V. S. Batista, *J. Chem. Phys.* **122**, 154709 (2005).
- ⁵¹K. Drukker, *J. Comput. Phys.* **153**, 225 (1999).
- ⁵²J. C. Tully, *Faraday Discuss.* **110**, 407 (1998).
- ⁵³J. C. Tully, *Int. J. Quantum Chem.* **40**, 299 (1991).
- ⁵⁴G. Granucci, M. Persico, and A. Zocante, *J. Chem. Phys.* **133**, 134111 (2010).
- ⁵⁵C. Y. Zhu, A. W. Jasper, and D. G. Truhlar, *J. Chem. Theory Comput.* **1**, 527 (2005).
- ⁵⁶J. E. Subotnik and N. Shenoi, *J. Chem. Phys.* **134**, 024105 (2011).
- ⁵⁷E. R. Bittner and P. J. Rossky, *J. Chem. Phys.* **103**, 8130 (1995).
- ⁵⁸W. Domcke, D. R. Yarkony, and H. Köppel, *Conical Intersections: Electronic Structure, Dynamics and Spectroscopy* (World Scientific, Singapore, 2004).
- ⁵⁹G. Stock and M. Thoss, *Adv. Chem. Phys.* **131**, 243 (2005).
- ⁶⁰H. B. Wang, X. Y. Song, D. Chandler, and W. H. Miller, *J. Chem. Phys.* **110**, 4828 (1999).
- ⁶¹H. D. Meyer, U. Manthe, and L. S. Cederbaum, *Chem. Phys. Lett.* **165**, 73 (1990).
- ⁶²M. H. Beck, A. Jackle, G. A. Worth, and H. D. Meyer, *Phys. Rep.* **324**, 1 (2000).
- ⁶³H. Tamura and I. Burghardt, *J. Am. Chem. Soc.* **135**, 16364 (2013).
- ⁶⁴H. D. Meyer and G. A. Worth, *Theor. Chem. Acc.* **109**, 251 (2003).
- ⁶⁵U. Manthe, *J. Chem. Phys.* **128**, 164116 (2008).
- ⁶⁶U. Manthe, *J. Chem. Phys.* **130**, 054109 (2009).
- ⁶⁷O. Vendrell and H.-D. Meyer, *J. Chem. Phys.* **134**, 044135 (2011).
- ⁶⁸Q. Meng and H.-D. Meyer, *J. Chem. Phys.* **138**, 014313 (2013).
- ⁶⁹Q. Meng, S. Faraji, O. Vendrell, and H.-D. Meyer, *J. Chem. Phys.* **137**, 134302 (2012).
- ⁷⁰G. A. Worth, M. H. Beck, A. Jackle, and H.-D. Meyer, The MCTDH package, version 8.2, University of Heidelberg, Heidelberg, Germany, 2000; H.-D. Meyer, The MCTDH package, version 8.3, 2002; The MCTDH package version 8.4, 2007; O. Vendrell and H.-D. Meyer, version 8.5, 2011, see <http://mctdh.uni-hd.de>.
- ⁷¹H. Köppel, W. Domcke, and L. S. Cederbaum, *Adv. Chem. Phys.* **57**, 59 (1984).
- ⁷²J. R. Li, M. Nilsing, I. Kondov, H. B. Wang, P. Persson, S. Lunell, and M. Thoss, *J. Phys. Chem. C* **112**, 12326 (2008).
- ⁷³W. Domcke, *Phys. Rep.* **208**, 97 (1991).
- ⁷⁴P. O. Löwdin, *J. Chem. Phys.* **18**, 365 (1950).
- ⁷⁵I. Mayer, *Int. J. Quantum Chem.* **90**, 63 (2002).
- ⁷⁶I. V. Kurnikov and D. N. Beratan, *J. Chem. Phys.* **105**, 9561 (1996).
- ⁷⁷M. Galperin, S. Toledo, and A. Nitzan, *J. Chem. Phys.* **117**, 10817 (2002).
- ⁷⁸TURBOMOLE V6.5 2013, a development of University of Karlsruhe and Forschungszentrum Karlsruhe GmbH, 1989-2007, TURBOMOLE GmbH, since 2007, available at: <http://www.turbomole.com>.
- ⁷⁹M. Sierka, A. Hogeckamp, and R. Ahlrichs, *J. Chem. Phys.* **118**, 9136 (2003).
- ⁸⁰M. J. Frisch, G. W. Trucks, H. B. Schlegel, G. E. Scuseria, M. A. Robb, J. R. Cheeseman, G. Scalmani, V. M. B. Barone, G. A. Petersson, H. Nakatsuji, M. Caricato, X. Li, H. P. Hratchian *et al.*, GAUSSIAN 09 (Gaussian, Inc., Wallingford, CT, 2009).
- ⁸¹See supplementary material at <http://dx.doi.org/10.1063/1.4909521> for the additional discussion on the quantum dynamics of different models (2S model, the inclusion of different vibrational modes, 4s model with other DFT functionals) obtained by various quantum propagation methods (standard quantum dynamics, MCTDH, ML-MCTDH), the dynamics at different temperatures, the dynamics with long-time propagation and relevant vibrational modes, etc.
- ⁸²M. D. Feit, J. A. Fleck, and A. Steiger, *J. Comput. Phys.* **47**, 412 (1982).

- ⁸³D. Kosloff and R. Kosloff, *J. Comput. Phys.* **52**, 35 (1983).
- ⁸⁴A. D. Isaacson and D. G. Truhlar, *J. Chem. Phys.* **80**, 2888 (1984).
- ⁸⁵A. Arnold and T. Jahnke, *BIT* **54**, 305 (2014).
- ⁸⁶R. D. Pensack, K. M. Banyas, and J. B. Asbury, *J. Phys. Chem. B* **114**, 12242 (2010).
- ⁸⁷M. Thoss, H. B. Wang, and W. H. Miller, *J. Chem. Phys.* **115**, 2991 (2001).
- ⁸⁸L. S. Cederbaum, E. Gindensperger, and I. Burghardt, *Phys. Rev. Lett.* **94**, 113003 (2005).
- ⁸⁹C. P. Hsu, *Acc. Chem. Res.* **42**, 509 (2009).
- ⁹⁰H. C. Chen, Z. Q. You, and C. P. Hsu, *J. Chem. Phys.* **129**, 084708 (2008).
- ⁹¹C. P. Hsu, Z. Q. You, and H. C. H. Chen, *J. Phys. Chem. C* **112**, 1204 (2008).
- ⁹²C.-P. Hsu, P. J. Walla, M. Head-Gordon, and G. R. Fleming, *J. Phys. Chem. B* **105**, 11016 (2001).
- ⁹³D. Ambrosek, A. Köhn, J. Schulze, and O. Kühn, *J. Phys. Chem. A* **116**, 11451 (2012).
- ⁹⁴J. E. Subotnik, R. J. Cave, R. P. Steele, and N. Shenvi, *J. Chem. Phys.* **130**, 234102 (2009).
- ⁹⁵J. E. Subotnik, S. Yeganeh, R. J. Cave, and M. A. Ratner, *J. Chem. Phys.* **129**, 244101 (2008).